

Supporting Information: Cavity-Modulated Proton Transfer Reactions

Fabijan Pavošević,^{*,†} Sharon Hammes-Schiffer,^{*,‡} Angel Rubio,^{*,¶,†,§} and

Johannes Flick^{*,†}

[†]*Center for Computational Quantum Physics, Flatiron Institute, 162 5th Ave., New York,
10010 NY, USA*

[‡]*Department of Chemistry, Yale University, 225 Prospect Street, New Haven, Connecticut,
06520, USA*

[¶]*Max Planck Institute for the Structure and Dynamics of Matter and Center for
Free-Electron Laser Science, Luruper Chaussee 149, 22761 Hamburg, Germany*

[§]*Nano-Bio Spectroscopy Group and European Theoretical Spectroscopy Facility (ETSF),
Universidad del País Vasco (UPV/EHU), Av. Tolosa 72, 20018 San Sebastian, Spain*

E-mail: fpavosevic@gmail.com; sharon.hammes-schiffer@yale.edu; angel.rubio@mpsd.mpg.de;
jflick@flatironinstitute.org

1 Theoretical Background

In general, interactions between molecules and photons inside an optical cavity can be described by the Pauli-Fierz Hamiltonian.¹⁻³ We include the optical cavity by coupling the electronic system to a single photon mode. We further employ the dipole approximation, since the wavelength of the photon mode is much larger than the extent of our molecular system and the length gauge,^{4,5} where the electric displacement field is coupled to the dipole moment of the system. Additionally we choose the coherent state basis.⁶ Under these assumptions, the Hamiltonian reads as follows (using atomic units unless otherwise stated)

$$\hat{H} = h_q^p a_p^q + \frac{1}{2} g_{rs}^{pq} a_{pq}^{rs} + \omega_{\text{cav}} b^\dagger b - \sqrt{\frac{\omega_{\text{cav}}}{2}} (\boldsymbol{\lambda} \cdot \Delta \mathbf{d}) (b^\dagger + b) + \frac{1}{2} (\boldsymbol{\lambda} \cdot \Delta \mathbf{d})^2 \quad (\text{S1})$$

We note that extensions to multi-mode setups, cavity losses,⁷ and correlation effects of nuclei^{8,9} are also possible. The first two terms constitute the electronic Hamiltonian within the Born-Oppenheimer approximation expressed in terms of the second-quantized electronic excitation operators $a_{p_1 p_2 \dots p_n}^{q_1 q_2 \dots q_n} = a_{q_1}^\dagger a_{q_2}^\dagger \dots a_{q_n}^\dagger a_{p_n} \dots a_{p_2} a_{p_1}$ that are defined as a string of fermionic creation and annihilation (a^\dagger and a , respectively) operators. Furthermore, $h_q^p = \langle q | \hat{h}^e | p \rangle$ and $g_{rs}^{pq} = \langle rs | \hat{h}^e | pq \rangle$ denote a matrix element of the core electronic Hamiltonian \hat{h}^e and a two-electron repulsion tensor element, respectively. The indices p, q, r, s, \dots denote general electronic spin orbitals, whereas indices i, j, k, l, \dots and a, b, c, d, \dots denote occupied and unoccupied electronic spin orbitals, respectively. The third term in this Hamiltonian denotes the photonic Hamiltonian for a single cavity mode with fundamental frequency ω_{cav} expressed in terms of bosonic creation/annihilation (b^\dagger/b) operators. The fourth term describes the dipolar coupling between the electrons and the photonic degrees of freedom. In this term, $\boldsymbol{\lambda}$ is the coupling strength vector that is connected to the field strength of the photon mode^{4,10} and depends, e.g., on the dielectric constant of the material inside the optical cavity and the quantization volume. The dipole fluctuation operator $\Delta \mathbf{d} = \mathbf{d} - \langle \mathbf{d} \rangle$ denotes the change of the dipole operator with respect to its expectation value. Note that the expectation value

of the dipole moment operator in the QED-CC approach is calculated at the QED-HF level, whereas we replace the dipole fluctuation operator by the dipole operator for the case of QEDFT. The molecular dipole operator $\mathbf{d} = \mathbf{d}_e + \mathbf{d}_{\text{nuc}}$ includes electronic and nuclear components. Finally, the last term in Eq. (S1) describes the dipole self energy arising in the length gauge.¹¹

In analogy to conventional electronic structure methods, there are two main ways for solving the Schrödinger equation that describes strong light-matter interaction, namely wave function and density functional based formalisms. In the following, we discuss the QED Hartree-Fock and coupled cluster methods, as well as the optimized-effective potential approach (OEP) for QEDFT in more detail.

In the quantum electrodynamics Hartree-Fock (QED-HF) method,^{6,12} the wave function ansatz is given as a direct product between an electronic Slater determinant $|0^e\rangle$ and a photon-number state $|0^{\text{ph}}\rangle$ as

$$|0^e 0^{\text{ph}}\rangle = |0^e\rangle \otimes |0^{\text{ph}}\rangle \quad (\text{S2})$$

where the superscripts e and ph denote electrons and photons, respectively. Due to the choice of the Hamiltonian in the coherent state basis, only the electronic orbitals are variationally optimized, and there is no need to further optimize the coherent photon state basis as described in detail in Ref. 6. Although the QED-HF method treats the electrons and photons as uncorrelated particles, it is a useful starting point for correlated methods. Among different approaches, in the QED-CC method⁶ the correlation effects between quantum particles (electrons and photons) are incorporated via the exponentiated cluster operator

$$\hat{T} = \sum_{\mu,n} t_{\mu,n} a^\mu (b^\dagger)^n \quad (\text{S3})$$

that acts on the reference QED-HF wave function as

$$|\Psi_{\text{QED-CC}}\rangle = e^{\hat{T}} |0^e 0^{\text{ph}}\rangle \quad (\text{S4})$$

In Eq. (S3), the amplitudes $t_{\mu,n}$ are unknown parameters that are determined by solving a set of nonlinear equations^{6,13,14}

$$\langle 0^e 0^{\text{ph}} | a_{\mu}(b)^n e^{-\hat{T}} \hat{H} e^{\hat{T}} | 0^e 0^{\text{ph}} \rangle = \sigma_{\mu,n} \quad (\text{S5})$$

Moreover, $a^{\mu} = a_{\mu}^{\dagger} = \{a_i^a, a_{ij}^{ab}, \dots\}$ is the electronic excitation operator, the index μ is the electronic excitation rank, and n denotes the number of photons. We also note that other choices of orbitals are possible, such as Kohn-Sham and Brueckner orbitals.¹⁵

The truncation of the cluster operator at a certain excitation rank μ and number of photons n establishes the QED-CC hierarchy. Truncation of the cluster operator to include up to single and double electronic excitations along with their interactions with a single photon is expressed as

$$\hat{T} = t_a^{i,0} a_i^a + t^{0,1} b^{\dagger} + \frac{1}{4} t_{ab}^{ij,0} a_{ij}^{ab} + t_a^{i,1} a_i^a b^{\dagger} + \frac{1}{4} t_{ab}^{ij,1} a_{ij}^{ab} b^{\dagger} \quad (\text{S6})$$

and defines the QED-CCSD-21 method introduced in Ref. 6. Note that the $-mn$ notation utilized throughout this paper denotes the highest degree of interactions of m electrons with n photons. We note here that at the onset of strong light-matter coupling, in Eq. (S6) the amplitude $t_a^{i,1}$ contributes the most. An extension of the cluster operator defined in Eq. (S6) to include up to two photons and their interactions with up to two electrons is expressed as

$$\hat{T} = t_a^{i,0} a_i^a + t^{0,1} b^{\dagger} + \frac{1}{4} t_{ab}^{ij,0} a_{ij}^{ab} + t_a^{i,1} a_i^a b^{\dagger} + \frac{1}{4} t_{ab}^{ij,1} a_{ij}^{ab} b^{\dagger} + t^{0,2} b^{\dagger} b^{\dagger} + t_a^{i,2} a_i^a b^{\dagger} b^{\dagger} + \frac{1}{4} t_{ab}^{ij,2} a_{ij}^{ab} b^{\dagger} b^{\dagger} \quad (\text{S7})$$

and defines the QED-CCSD-22 method introduced in Ref. 16. Lastly, truncation of the cluster operator to include interactions between only one electron with up to two photons is expressed as

$$\hat{T} = t_a^{i,0} a_i^a + t^{0,1} b^{\dagger} + \frac{1}{4} t_{ab}^{ij,0} a_{ij}^{ab} + t_a^{i,1} a_i^a b^{\dagger} + t^{0,2} b^{\dagger} b^{\dagger} + t_a^{i,2} a_i^a b^{\dagger} b^{\dagger} \quad (\text{S8})$$

and defines the QED-CCSD-12 method first introduced in Ref. 17 in the context of the description of the electron-phonon interaction. Because the computational cost of the QED-CCSD- mn methods is determined by the number of $t_{ab}^{ij,n}$ amplitude equations that need to be solved, the computational cost of the QED-CCSD-21 and QED-CCSD-22 methods are roughly two and three times higher, respectively, than the computational cost of the QED-CCSD-12 method.

Next, we briefly discuss the optimized-effective potential approach^{10,18} to QEDFT. In contrast to the wave function based methods, such as QED-HF and QED-CC, the QEDFT method obtains solutions to the Schrödinger equation including quantized light-matter interactions in Eq. (S1) in terms of reduced quantities (internal variables). In the length-gauge and dipole approximations, convenient choices for these internal variables are the electron density $n(\mathbf{r})$ and the photon displacement coordinate $q = \sqrt{\frac{\hbar}{2\omega_{\text{cav}}}} (b^\dagger + b)$.^{1,2} Although QEDFT is in principle exact, for practical calculations approximations to the so-called exchange-correlation (xc) potential need to be specified. For QEDFT, these xc potentials must capture not only the correlated nature of the electron-electron interaction as in regular DFT, but also the correlated nature of the quantized electron-photon interaction. So far only a few approximations are available, either in terms of orbital functionals^{10,18} or density functionals.^{19,20} In this work, we choose the optimized-effective potential approximation, which was the first xc potential introduced for QEDFT and is the most established xc potential for problems in QEDFT. This approach is based on the following exchange-correlation energy,^{10,18} which reads for a single photon mode as follows:

$$E_{xc}^{(OEP)} = -\frac{1}{2} \sum_{i,a} |\langle \varphi_i | \boldsymbol{\lambda} \cdot \Delta \mathbf{d} | \varphi_a \rangle|^2 \left(\frac{\omega_{\text{cav}}}{\epsilon_a - \epsilon_i + \omega_{\text{cav}}} - 1 \right) \quad (\text{S9})$$

where ϵ_i and ϵ_a denote occupied and unoccupied Kohn-Sham orbital energies, respectively. We note that the energy expression in Eq. (S9) includes occupied and unoccupied orbitals, but an efficient reformulation in terms of only occupied orbitals is also possible.¹⁸ This

approximation, which is referred to as one-photon OEP, explicitly accounts for one-photon absorption and emission effects and has been shown to be accurate in the weak and strong light-matter coupling regimes.^{10,18,21} For more details on the one-photon OEP approach, we refer the reader to Refs. 10,18,21–23.

2 Computational Details

The QED-CCSD-*mn* methods have been implemented in an in-house developmental version of the Psi4NumPy quantum chemistry software.²⁴ The implemented QED-CCSD-*mn* methods, along with the QEDFT method, were used to calculate the reaction energy diagrams for proton transfer in malonaldehyde and aminopropenal. All calculations were performed on the geometries optimized at the conventional electronic CCSD/cc-pVDZ²⁵ level using the Gaussian quantum chemistry software,²⁶ and the optimized geometries are provided below. The geometry optimizations were performed using the standard optimization procedures^{27,28} with default parameters as implemented in Gaussian 16.²⁶ The characters of the stationary structures on the potential energy surface (i.e., reactants, transition states, and products) were confirmed by performing the harmonic frequency analysis. We note however, that the stationary points can be different between HF, CCSD, and DFT. The QED-HF and the QED-CCSD-*mn* calculations were performed by employing the cc-pVDZ basis set.²⁵

The QEDFT calculations were performed using the Octopus code²² with the single-photon OEP implementation described in Refs. 18,22. This formulation describes both the electron-electron interaction and the electron-photon interaction consistently within the OEP approach. If no electron-photon coupling is present, this approach reduces to the electronic OEP framework.²⁹ In all calculations with the Octopus code, we used a real-space grid with spheres of 6 Å around each atom and a grid spacing of 0.15 Å to be consistent with previous work,^{19,21} as well as Troullier-Martins pseudopotentials³⁰ to describe the core electrons.

3 Estimation of the Molecular Volume

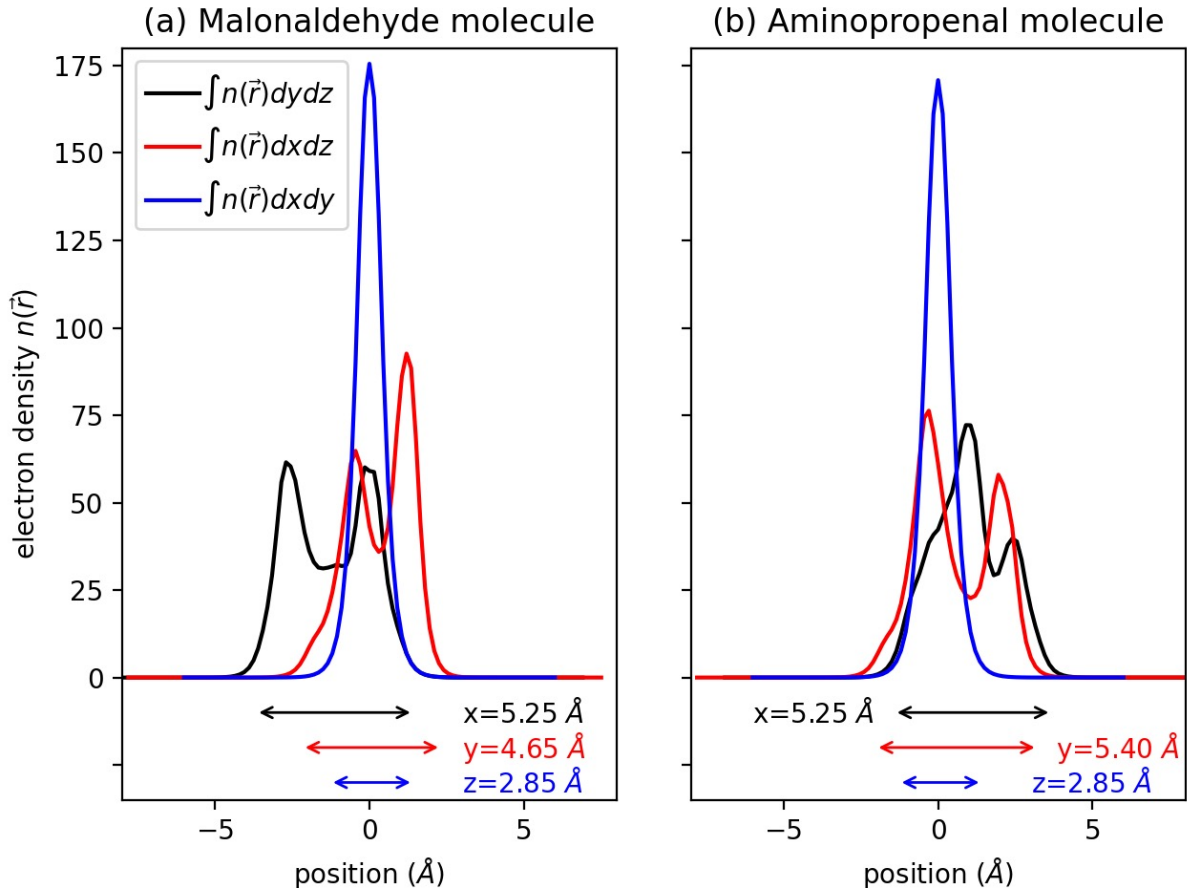


Figure S1: Spread of the electron density for the (a) malonaldehyde and (b) aminopropenal molecules in an OEP calculation at the reactant geometry

. The orthogonal axes have been traced out for each direction.

In this section, we estimate the volume occupied by the molecule via the spread of the ground-state electron density. In Fig. S1, we visualize the electron density of the malonaldehyde and aminopropenal molecules in the reactant geometry for an OEP calculation outside an optical cavity. In the figure, we show the electron density along the x , y , and z axes, where the orthogonal axes have been traced out for each direction. The arrows in the figure specify the spread of the electron density, such that $\sim 99\%$ of the electron density falls inside the area specified by the arrow. Using this methodology, we can estimate a volume of $V_{\text{mol}} = 0.070 \text{ nm}^3$ for the malonaldehyde molecule and $V_{\text{mol}} = 0.081 \text{ nm}^3$ for the aminopropenal molecule.

4 Rabi Splitting for Different Electron-photon Coupling Strengths

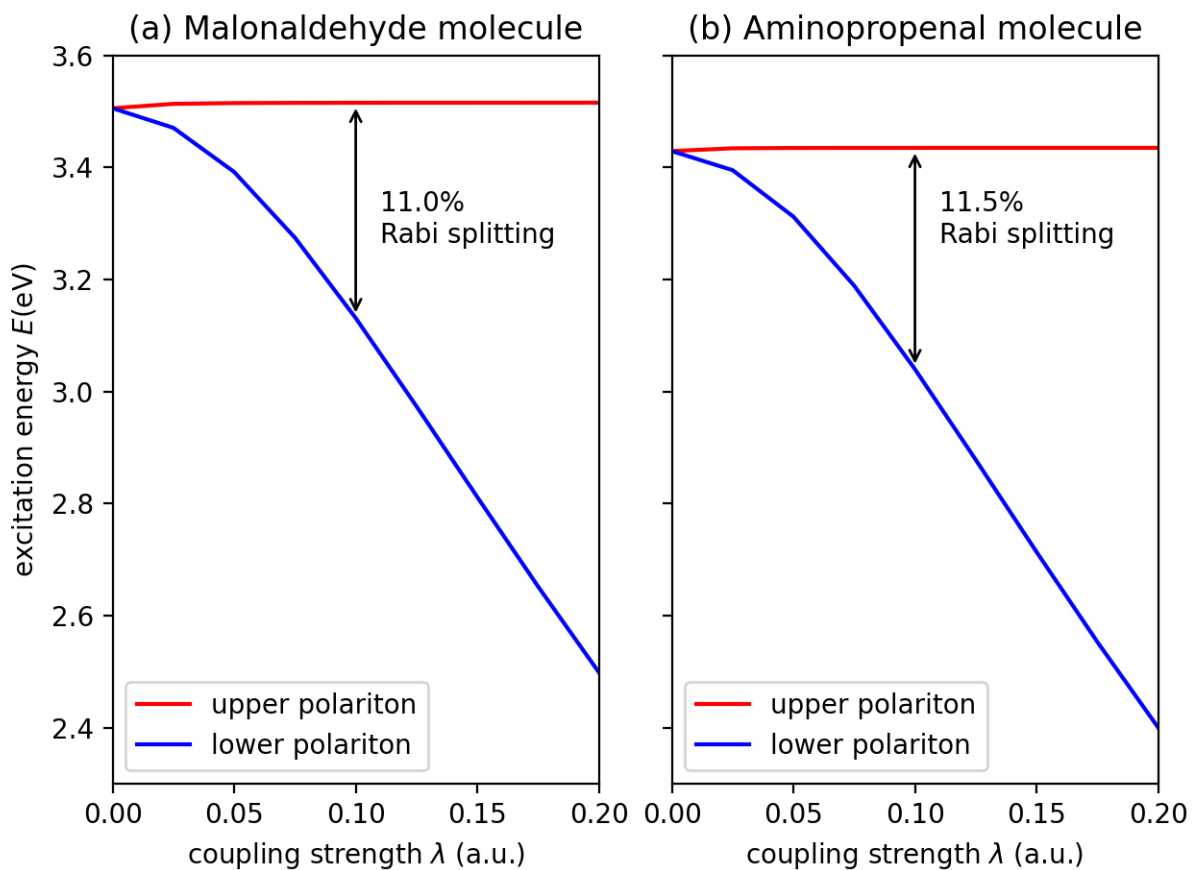


Figure S2: Excitation energies of the upper polariton (UP) (red) and lower polariton (LP) (blue) for the (a) malonaldehyde and (b) aminopropenal molecules as a function of the coupling strength $\lambda = [0, 0, \lambda]$ a.u. The calculations employ a cavity frequency of $\omega_{\text{cav}} = 3.51$ eV and $\omega_{\text{cav}} = 3.43$ eV in resonance with their respective HOMO-LUMO excitation energy of the malonaldehyde and aminopropenal molecules.

In this section, we calculate the Rabi splitting for malonaldehyde and aminopropenal, since the ratio of the Rabi splitting to the cavity frequency is routinely used as a measure of the strong coupling regime.³¹ Figure S2 shows the energy of the lower and upper polariton as a function of the coupling strength for the malonaldehyde and the aminopropenal molecules. The energy difference between the lower and upper polariton yields the Rabi splitting. The

cavity frequency of $\omega_{\text{cav}} = 3.51$ eV for the malonaldehyde molecule and $\omega_{\text{cav}} = 3.43$ eV for the aminopropenal molecule are in resonance with their respective HOMO-LUMO excitations, leading to hybrid light-matter (polariton) states in this energy range. The coupling strength vector is chosen along the z direction (perpendicular to the molecular plane), i.e., $\boldsymbol{\lambda} = [0, 0, \lambda]$ a.u., since the HOMO-LUMO excitations of both molecules have the highest transition dipole moment in that direction. We find that for the coupling strength of $\lambda = 0.1$ a.u. the ratio of the Rabi splitting to the cavity frequency is 11-12%, which is within the range of experimentally observed values in the single-molecule³² and collective strong coupling³³ limits. In this calculation of polaritonic excited states, we employ the linear response QEDFT method³⁴ together with the LDA exchange-correlation potential^{35,36} to describe the electron-electron interactions using the reactant geometry. We employ 100 unoccupied states in the linear-response calculation, and the calculation outside the optical cavity yields HOMO-LUMO transition energies of 3.51 eV for malonaldehyde and 3.43 eV for aminopropenal. All other parameters are chosen as described in the main manuscript.

5 Change in the Reaction Energy Barrier for Proton Transfer in Malonaldehyde inside an Optical Cavity with Cavity Parameters $\lambda = 0.1$ a.u. and $\omega = 3$ eV at Geometry Optimized with Hartree-Fock

Table S1: Change in the Reaction Energy Barrier (TS) for Proton Transfer in Malonaldehyde inside an Optical Cavity.^a

method	<i>x</i> direction	<i>y</i> direction	<i>z</i> direction
QED-HF	1.37	0.27	-0.05
QED-CCSD-12	1.12	0.15	-0.28
QED-CCSD-21	0.99	0.08	-0.28
QED-CCSD-22	0.94	0.06	-0.28
QEDFT(OEP)	0.87	0.05	0.01

^aRelative energies are calculated as the difference between the reaction barrier obtained with the QED method and the corresponding conventional electronic structure method (difference between the QED and the non-QED calculation). Relative energies are given in kcal/mol.

Table S1 shows the changes in reaction barriers for the cavity mode polarized along the *x*, *y*, and *z* directions calculated with all of the QED methods using the reactant and transition state geometries optimized with the HF/cc-pVDZ method. By comparing Table S1 and Table 1, it is evident that the trends of the cavity effects are not significantly influenced by these geometrical differences.

6 Energy Contributions Breakdown

Table S2: Energy Contributions to Reaction Energy Barrier (in kcal/mol) for Proton Transfer Reaction in Malonaldehyde Obtained with Different QED-CCSD- mn Methods.

	outside cavity	x-direction		y-direction		z-direction	
	QED-CCSD-12						
energy contributions	0 eV	0 eV	3 eV	0 eV	3 eV	0 eV	3 eV
electronic	5.19	5.68	5.67	5.43	5.42	5.16	5.17
dipole self energy	0.00	0.65	0.66	-0.08	-0.08	-0.21	-0.21
dipolar coupling	0.00	0.00	-0.14	0.00	-0.03	0.00	-0.01
QED-CCSD-12	5.19	6.33	6.20	5.35	5.31	4.96	4.94
	QED-CCSD-21						
energy contributions	0 eV	0 eV	3 eV	0 eV	3 eV	0 eV	3 eV
electronic	5.19	5.68	5.64	5.43	5.42	5.16	5.17
dipole self energy	0.00	0.65	0.66	-0.08	-0.08	-0.21	-0.21
dipolar coupling	0.00	0.00	-0.23	0.00	-0.10	0.00	-0.01
QED-CCSD-21	5.19	6.33	6.08	5.35	5.24	4.96	4.95
	QED-CCSD-22						
energy contributions	0 eV	0 eV	3 eV	0 eV	3 eV	0 eV	3 eV
electronic	5.19	5.68	5.64	5.43	5.42	5.16	5.17
dipole self energy	0.00	0.65	0.67	-0.08	-0.07	-0.21	-0.21
dipolar coupling	0.00	0.00	-0.29	0.00	-0.11	0.00	-0.01
QED-CCSD-22	5.19	6.33	6.01	5.35	5.23	4.96	4.95

Table S2 shows the energy contributions to the reaction energy barrier of the proton transfer reaction in the malonaldehyde molecule obtained with the different QED-CCSD- mn (QED-HF + correlation) methods. The three energy contributions are electronic $\left(\langle 0^e 0^{\text{ph}} | \hat{H}^e | 0^e 0^{\text{ph}} \rangle + \bar{g}_{ij}^{ab} \times (0.25 \cdot t_{ab}^{ij,0} + 0.5 \cdot t_a^{i,0} t_b^{j,0}) \right)$, dipole self energy $\left(\langle 0^e 0^{\text{ph}} | \frac{1}{2} (\boldsymbol{\lambda} \cdot \Delta \mathbf{d})^2 | 0^e 0^{\text{ph}} \rangle + ((\boldsymbol{\lambda} \cdot \mathbf{d})_{ij}^{ab})^2 \times (0.25 \cdot t_{ab}^{ij,0} + 0.5 \cdot t_a^{i,0} t_b^{j,0}) \right)$, and dipolar coupling $\left((\boldsymbol{\lambda} \cdot \mathbf{d})_i^a \times (t_a^{i,1} + t_a^{i,0} t^{0,1}) \right)$. The calculations employ cavity parameters $\lambda = 0.0$ (outside cavity) and $\lambda = 0.1$ a.u. (inside cavity), with cavity frequency of 0 eV and 3 eV. Table S2 shows that for $\omega_{\text{cav}} = 0$ eV the dipolar coupling does not contribute to the total energy. Since the QED-CCSD- mn methods are only different in how they treat the electron-photon interaction, they yield the same value when $\omega_{\text{cav}} = 0$ eV. The dipolar coupling contributes to the total correlation energy only for $\omega_{\text{cav}} > 0$ eV, which is where the different QED-CCSD- mn methods differ.

7 Energy Barrier Dependence on the Cavity Frequency with the Cavity Mode Polarized Along the x Direction

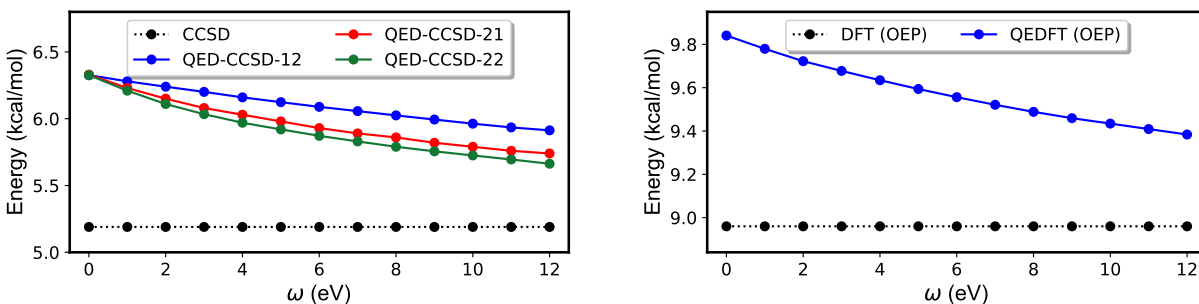


Figure S3: Proton transfer reaction barrier for malonaldehyde as a function of cavity frequency. Dotted lines correspond to calculations outside the cavity, whereas solid lines correspond to calculations inside the cavity with the cavity mode polarized along the x direction and with coupling strength 0.1 a.u. Reaction barriers calculated with the conventional CCSD and DFT methods, along with their QED counterparts, are given in the left and right panels, respectively.

Figure S3 shows the change in the reaction barrier for malonaldehyde calculated with the CCSD methods (left panel) and the DFT methods (right panel) as the cavity frequency is increased from 0 eV to 12 eV by 1 eV increments. The QED barriers (solid lines) were calculated in a cavity with the mode polarized along the x direction with coupling strength 0.1 a.u. The reaction barrier energies calculated with the conventional CCSD and DFT methods are depicted with the dotted black line and are independent of the cavity frequency. We find that the QED-CCSD-21 method is in good agreement with the QED-CCSD-22 method for all values of ω_{cav} , whereas the QED-CCSD-12 method deviates more significantly relative to the QED-CCSD-22 method. Thus, the QED-CCSD-12 method should be used with caution in the case of large cavity frequencies.

8 Cartesian Coordinates of the Optimized Geometries

Optimized with HF/cc-pVDZ method:

Malonaldehyde Reactant (Number of Imaginary Frequencies=0)

C	0.00000000	0.00000000	0.00000000
O	0.00000000	1.20455422	0.00000000
H	0.95734071	-0.54243020	0.00000000
C	-1.20383213	-0.81852146	0.00000000
H	-1.11979107	-1.89455068	0.00000000
C	-2.42275525	-0.24888403	0.00000000
H	-3.32308880	-0.85121280	0.00000000
O	-2.67738957	1.03726336	0.00000000
H	-1.84616630	1.51635779	0.00000000

Optimized with HF/cc-pVDZ method:

Malonaldehyde Transition State (Number of Imaginary Frequencies=1)

C	0.00000000	0.00000000	0.00000000
O	0.00000000	1.25379443	0.00000000
H	0.96967882	-0.49901661	0.00000000
C	-1.18350394	-0.74049865	0.00000000
H	-1.19360917	-1.81729824	0.00000000
C	-2.35311485	0.02202151	0.00000000
H	-3.33189033	-0.45893666	0.00000000
O	-2.32977945	1.27553951	0.00000000
H	-1.16257041	1.51073704	0.00000000

Optimized with CCSD/cc-pVDZ method:

Malonaldehyde Reactant (Number of Imaginary Frequencies=0)

C	0.00000000	0.00000000	0.00000000
O	0.00000000	1.23456800	0.00000000
H	0.97075033	-0.54577032	0.00000000
C	-1.21509881	-0.80991169	0.00000000
H	-1.15288176	-1.89931439	0.00000000
C	-2.43440063	-0.19144555	0.00000000
H	-3.37262777	-0.75937214	0.00000000
O	-2.62194056	1.12501165	0.00000000
H	-1.71446384	1.51627790	0.00000000

Optimized with CCSD/cc-pVDZ method:

Malonaldehyde Transition State (Number of Imaginary Frequencies=1)

C	0.00000000	0.00000000	0.00000000
O	0.00000000	1.27847000	0.00000000
H	0.98371462	-0.50070158	0.00000000
C	-1.19326902	-0.74784832	0.00000000
H	-1.19970349	-1.83682931	0.00000000
C	-2.37814431	0.01400581	0.00000000
H	-3.36752991	-0.47550725	0.00000000
O	-2.36325335	1.29201906	0.00000000
H	-1.17975465	1.50752679	0.00000000

Optimized with CCSD/cc-pVDZ method:

Aminopropenal Reactant (Number of Imaginary Frequencies=0)

H	0.00000000	0.00000000	0.00000000
C	0.00000000	1.09163906	0.00000000

C	1.26822472	1.80690645	0.00000000
N	-1.33404678	3.10992888	0.00000000
O	1.39279087	3.03379031	0.00000000
H	-0.48254004	3.66582880	0.00000000
H	-2.24599052	3.54003736	0.00000000
C	-1.19931821	1.76513995	0.00000000
H	2.18220599	1.16371496	0.00000000
H	-2.14055701	1.20128576	0.00000000

Optimized with CCSD/cc-pVDZ method:

Aminopropenal Transition State (Number of Imaginary Frequencies=1)

H	0.00000000	0.00000000	0.00000000
C	0.00000000	1.08943910	0.00000000
C	1.19187861	1.82073020	0.00000000
N	-1.15503519	3.15085322	0.00000000
O	1.23956085	3.10723950	0.00000000
H	0.06714025	3.42106531	0.00000000
H	-2.03971004	3.65182794	0.00000000
C	-1.21230682	1.83679656	0.00000000
H	2.16133262	1.29142618	0.00000000
H	-2.18458586	1.32025952	0.00000000

Optimized with CCSD/cc-pVDZ method:

Aminopropenal Product (Number of Imaginary Frequencies=0)

H	0.00000000	0.00000000	0.00000000
C	0.00000000	1.09138840	0.00000000
C	1.19000326	1.75971354	0.00000000
N	-1.29869978	3.11237163	0.00000000

O	1.33369004	3.08569523	0.00000000
H	0.41141507	3.45367072	0.00000000
H	-2.26092059	3.46346742	0.00000000
C	-1.27014745	1.81619151	0.00000000
H	2.14625767	1.22260226	0.00000000
H	-2.19412100	1.21051211	0.00000000

References

- (1) Ruggenthaler, M.; Flick, J.; Pellegrini, C.; Appel, H.; Tokatly, I. V.; Rubio, A. Quantum-Electrodynamical Density-Functional Theory: Bridging Quantum Optics and Electronic-Structure Theory. *Phys. Rev. A* **2014**, *90*, 012508.
- (2) Tokatly, I. V. Time-Dependent Density Functional Theory for Many-Electron Systems Interacting with Cavity Photons. *Phys. Rev. Lett.* **2013**, *110*, 233001.
- (3) Ruggenthaler, M.; Tancogne-Dejean, N.; Flick, J.; Appel, H.; Rubio, A. From a Quantum-Electrodynamical Light-Matter Description to Novel Spectroscopies. *Nat. Rev. Chem.* **2018**, *2*, 1–16.
- (4) Craig, D.; Thirunamachandran, T. *Molecular Quantum Electrodynamics: An Introduction to Radiation-molecule Interactions*; Dover Books on Chemistry Series; Dover Publications, 1998.
- (5) Schäfer, C.; Ruggenthaler, M.; Rokaj, V.; Rubio, A. Relevance of the Quadratic Diamagnetic and Self-polarization Terms in Cavity Quantum Electrodynamics. *ACS Photonics* **2020**, *7*, 975–990.
- (6) Haugland, T. S.; Ronca, E.; Kjørstad, E. F.; Rubio, A.; Koch, H. Coupled Cluster

- Theory for Molecular Polaritons: Changing Ground and Excited States. *Phys. Rev. X* **2020**, *10*, 041043.
- (7) Wang, D. S.; Neuman, T.; Flick, J.; Narang, P. Light–matter Interaction of a Molecule in a Dissipative Cavity from First Principles. *J. Chem. Phys.* **2021**, *154*, 104109.
- (8) Pavošević, F.; Culpitt, T.; Hammes-Schiffer, S. Multicomponent Coupled Cluster Singles and Doubles Theory within the Nuclear-Electronic Orbital Framework. *J. Chem. Theory Comput.* **2019**, *15*, 338–347.
- (9) Pavošević, F.; Culpitt, T.; Hammes-Schiffer, S. Multicomponent Quantum Chemistry: Integrating Electronic and Nuclear Quantum Effects via the Nuclear-Electronic Orbital Method. *Chem. Rev.* **2020**, *120*, 4222–4253.
- (10) Pellegrini, C.; Flick, J.; Tokatly, I. V.; Appel, H.; Rubio, A. Optimized Effective Potential for Quantum Electrodynamical Time-Dependent Density Functional Theory. *Phys. Rev. Lett.* **2015**, *115*, 093001.
- (11) Rokaj, V.; Welakuh, D. M.; Ruggenthaler, M.; Rubio, A. Light–matter Interaction in the Long-wavelength Limit: No Ground-state Without Dipole Self-energy. *J. Phys. B* **2018**, *51*, 034005.
- (12) Rivera, N.; Flick, J.; Narang, P. Variational Theory of Nonrelativistic Quantum Electrodynamics. *Phys. Rev. Lett.* **2019**, *122*, 193603.
- (13) Bartlett, R. J.; Musiał, M. Coupled-Cluster Theory in Quantum Chemistry. *Rev. Mod. Phys.* **2007**, *79*, 291.
- (14) Shavitt, I.; Bartlett, R. J. *Many-Body Methods in Chemistry and Physics: MBPT and Coupled-Cluster Theory*; Cambridge University Press, 2009.
- (15) Fang, Z.; Lee, Z.; Peterson, K. A.; Dixon, D. A. Use of Improved Orbitals for CCSD(T)

- Calculations for Predicting Heats of Formation of Group IV and Group VI Metal Oxide Monomers and Dimers and UCl₆. *J. Chem. Theory Comput.* **2016**, *12*, 3583–3592.
- (16) Pavošević, F.; Flick, J. Polaritonic Unitary Coupled Cluster for Quantum Computations. *J. Phys. Chem. Lett.* **2021**, *12*, 9100–9107.
- (17) White, A. F.; Gao, Y.; Minnich, A. J.; Chan, G. K.-L. A Coupled Cluster Framework for Electrons and Phonons. *J. Chem. Phys.* **2020**, *153*, 224112.
- (18) Flick, J.; Schäfer, C.; Ruggenthaler, M.; Appel, H.; Rubio, A. Ab Initio Optimized Effective Potentials for Real Molecules in Optical Cavities: Photon Contributions to the Molecular Ground State. *ACS Photonics* **2018**, *5*, 992–1005.
- (19) Flick, J. Simple Exchange-Correlation Energy Functionals for Strongly Coupled Light-Matter Systems based on the Fluctuation-Dissipation Theorem. *arXiv:2104.06980 (Physics.Chemical Physics)* **April 14 2021**, <https://doi.org/10.48550/arXiv.2104.06980>.
- (20) Schäfer, C.; Buchholz, F.; Penz, M.; Ruggenthaler, M.; Rubio, A. Making ab initio QED Functional (s): Non-perturbative and Photon-free Effective Frameworks for Strong Light-matter Coupling. *Proc. Natl. Acad. Sci. U.S.A.* **2021**, *118*, e2110464118.
- (21) Haugland, T. S.; Schäfer, C.; Ronca, E.; Rubio, A.; Koch, H. Intermolecular Interactions in Optical Cavities: An Ab Initio QED Study. *J. Chem. Phys.* **2021**, *154*, 094113.
- (22) Tancogne-Dejean, N.; Oliveira, M. J. T.; Andrade, X.; Appel, H.; Borca, C. H.; Le Breton, G.; Buchholz, F.; Castro, A.; Corni, S.; Correa, A. A.; De Giovannini, U.; Delgado, A.; Eich, F. G.; Flick, J.; Gil, G.; Gomez, A.; Helbig, N.; Hübener, H.; Jestädt, R.; Jornet-Somoza, J.; Larsen, A. H.; Lebedeva, I. V.; Lüders, M.; Marques, M. A. L.; Ohlmann, S. T.; Pipolo, S.; Rampp, M.; Rozzi, C. A.; Strubbe, D. A.; Sato, S. A.; Schäfer, C.; Theophilou, I.; Welden, A.; Rubio, A. Octopus, a Computational Frame-

- work for Exploring Light-driven Phenomena and Quantum Dynamics in Extended and Finite Systems. *J. Chem. Phys.* **2020**, *152*, 124119.
- (23) Schäfer, C. On the interface of quantum electrodynamics and electronic structure theory: Cavity QED. Ph.D. thesis, Universität Hamburg Hamburg, 2020.
- (24) Smith, D. G.; Burns, L. A.; Sirianni, D. A.; Nascimento, D. R.; Kumar, A.; James, A. M.; Schriber, J. B.; Zhang, T.; Zhang, B.; Abbott, A. S., et al. Psi4NumPy: An Interactive Quantum Chemistry Programming Environment for Reference Implementations and Rapid Development. *J. Chem. Theory Comput.* **2018**, *14*, 3504–3511.
- (25) Dunning Jr, T. H. Gaussian Basis Sets for use in Correlated Molecular Calculations. I. The Atoms Boron through Neon and Hydrogen. *J. Chem. Phys.* **1989**, *90*, 1007–1023.
- (26) Frisch, M. J.; Trucks, G. W.; Schlegel, H. B.; Scuseria, G. E.; Robb, M. A.; Cheeseman, J. R.; Scalmani, G.; Barone, V.; Petersson, G. A.; Nakatsuji, H.; Li, X.; Caricato, M.; Marenich, A. V.; Bloino, J.; Janesko, B. G.; Gomperts, R.; Mennucci, B.; Hratchian, H. P.; Ortiz, J. V.; Izmaylov, A. F.; Sonnenberg, J. L.; Williams-Young, D.; Ding, F.; Lipparini, F.; Egidi, F.; Goings, J.; Peng, B.; Petrone, A.; Henderson, T.; Ranasinghe, D.; Zakrzewski, V. G.; Gao, J.; Rega, N.; Zheng, G.; Liang, W.; Hada, M.; Ehara, M.; Toyota, K.; Fukuda, R.; Hasegawa, J.; Ishida, M.; Nakajima, T.; Honda, Y.; Kitao, O.; Nakai, H.; Vreven, T.; Throssell, K.; Montgomery, J. A., Jr.; Peralta, J. E.; Ogliaro, F.; Bearpark, M. J.; Heyd, J. J.; Brothers, E. N.; Kudin, K. N.; Staroverov, V. N.; Keith, T. A.; Kobayashi, R.; Normand, J.; Raghavachari, K.; Rendell, A. P.; Burant, J. C.; Iyengar, S. S.; Tomasi, J.; Cossi, M.; Millam, J. M.; Klene, M.; Adamo, C.; Cammi, R.; Ochterski, J. W.; Martin, R. L.; Morokuma, K.; Farkas, O.; Foresman, J. B.; Fox, D. J. Gaussian 16 Revision A.03. Gaussian Inc. Wallingford CT 2016.

- (27) Schlegel, H. B. Optimization of Equilibrium Geometries and Transition Structures. *J. Comput. Chem.* **1982**, *3*, 214–218.
- (28) Peng, C.; Bernhard Schlegel, H. Combining Synchronous Transit and Quasi-newton Methods to find Transition States. *Isr. J. Chem.* **1993**, *33*, 449–454.
- (29) Kümmel, S.; Kronik, L. Orbital-dependent Density Functionals: Theory and Applications. *Rev. Mod. Phys.* **2008**, *80*, 3–60.
- (30) Troullier, N.; Martins, J. L. Efficient Pseudopotentials for Plane-wave Calculations. *Phys. Rev. B* **1991**, *43*, 1993–2006.
- (31) Casanova, J.; Romero, G.; Lizuain, I.; García-Ripoll, J. J.; Solano, E. Deep Strong Coupling Regime of the Jaynes-Cummings Model. *Phys. Rev. Lett.* **2010**, *105*, 263603.
- (32) Chikkaraddy, R.; de Nijs, B.; Benz, F.; Barrow, S. J.; Scherman, O. A.; Rosta, E.; Demetriadou, A.; Fox, P.; Hess, O.; Baumberg, J. J. Single-molecule Strong Coupling at Room Temperature in Plasmonic Nanocavities. *Nature* **2016**, *535*, 127–130.
- (33) Hutchison, J. A.; Schwartz, T.; Genet, C.; Devaux, E.; Ebbesen, T. W. Modifying Chemical Landscapes by Coupling to Vacuum Fields. *Angew. Chem.* **2012**, *51*, 1592–1596.
- (34) Flick, J.; Welakuh, D. M.; Ruggenthaler, M.; Appel, H.; Rubio, A. Light–Matter Response in Nonrelativistic Quantum Electrodynamics. *ACS Photonics* **2019**, *6*, 2757–2778.
- (35) Hohenberg, P.; Kohn, W. Inhomogeneous Electron Gas. *Phys. Rev.* **1964**, *136*, B864.
- (36) Perdew, J. P.; Zunger, A. Self-interaction correction to density-functional approximations for many-electron systems. *Phys. Rev. B* **1981**, *23*, 5048–5079.